

Underlying Physical Mechanisms in Upward Positive Flashes

T. Oregel-Chaumont¹, A. Šunjerga², J. Kasparian³, M. Rubinstein⁴, and F. Rachidi¹

¹EPFL

²University of Split

³University of Geneva

⁴HEIG-VD

Key Points:

- We present the first observation of a mixed-mode of charge transfer during an upward positive flash.
- The triggering positive recoil leader exhibited step-like behaviour, also a novel observation.
- The findings challenge existing classifications for mixed mode and M-component-type pulses, suggesting a continuous charge transfer mode.

arXiv:2501.08110v1 [physics.plasm-ph] 14 Jan 2025

Abstract

This study presents the first observation of a mixed mode of charge transfer during an upward positive flash, which was initiated from the Säntis Tower in Switzerland. High-speed camera footage, along with current and electric field measurements, revealed a downward-propagating recoil leader connecting to the grounded current-carrying plasma channel at a junction height of <1 km above the tip of the tower. This event triggered the “return stroke”-like main pulse associated with Type 1 upward positive flashes, leading us to propose a mixed mode of charge transfer (normally observed in upward *negative* flashes) as the physical mechanism at play. Furthermore, the observed pulse shared characteristics with both mixed-mode and M-component -type initial continuous current (ICC) pulses, challenging existing classification criteria, and supporting the notion of a singular mode of charge transfer with a range of junction-dependent pulse characteristics, as opposed to two distinct modes. The recoil leader itself was accompanied by a sequence of fast electric field pulses indicative of step-like propagation, also an observational first. These findings contribute to improving our understanding of the mechanisms of charge transfer in upward lightning flashes.

Plain Language Summary

Despite its ubiquitous nature, lightning is a complex phenomenon that scientists are still working to understand fully. In addition to the more common downward, cloud-to-ground strikes, lightning can also propagate *upwards*, typically from the tips of tall towers, wind turbines, or airplanes, and can exchange both positive *and/or* negative charge in the process. This study discusses a particular upward positive flash that occurred at the Säntis Tower in Switzerland. Using high-speed camera footage, electric field sensors, and a current measurement system, the researchers were able to determine that this flash experienced a simultaneous exchange of both positive and negative charge, known as a “mixed-mode”, during part of its duration, which manifested itself as brightening of the main lightning branch in the video, accompanied by large pulses in the current and electric field records. This was the first time that such a mode was observed in an upward positive flash, and challenges existing notions about how charge is transferred during upward lightning in general. Lightning protection systems are usually designed to deal with downward flashes exclusively, making this discovery particularly relevant, as upward flashes become more frequent with the continued construction of strike-prone objects.

1 Introduction

The term “mixed mode” of charge transfer to ground for ICC pulses in the context of upward lightning flashes was first proposed by Zhou et al. (2011) to describe fast pulses, distinct from the classical M-component mode of charge transfer (e.g., Rakov et al. (1995) and Azadifar et al. (2019)), superimposed on the slowly varying initial-stage current of upward negative flashes. The pulses in question were associated with processes similar to leader/return-stroke events occurring in decayed or newly-created branches of the plasma channel connecting to the grounded, current-carrying channel, with junction points below the cloud base (height <1 km AGL, as opposed to M-Component-type ICC pulses with junction heights above 1 km) (Zhou et al., 2015). “Mixed-mode” was coined specifically due to the observed presence of two distinct channels with a common section, involving different charge transfer modes. In addition to this junction point height cutoff they defined at ~ 1 km, three other criteria have also been proposed in the literature to distinguish M-component-type ICC pulses and mixed-mode pulses (Li et al., 2023): the lag between the channel-base current pulse and its associated radiated electric field pulse (Zhou et al., 2015), the current pulse rise time (Flache et al., 2008), and the pulse waveform asymmetry (He et al., 2018).

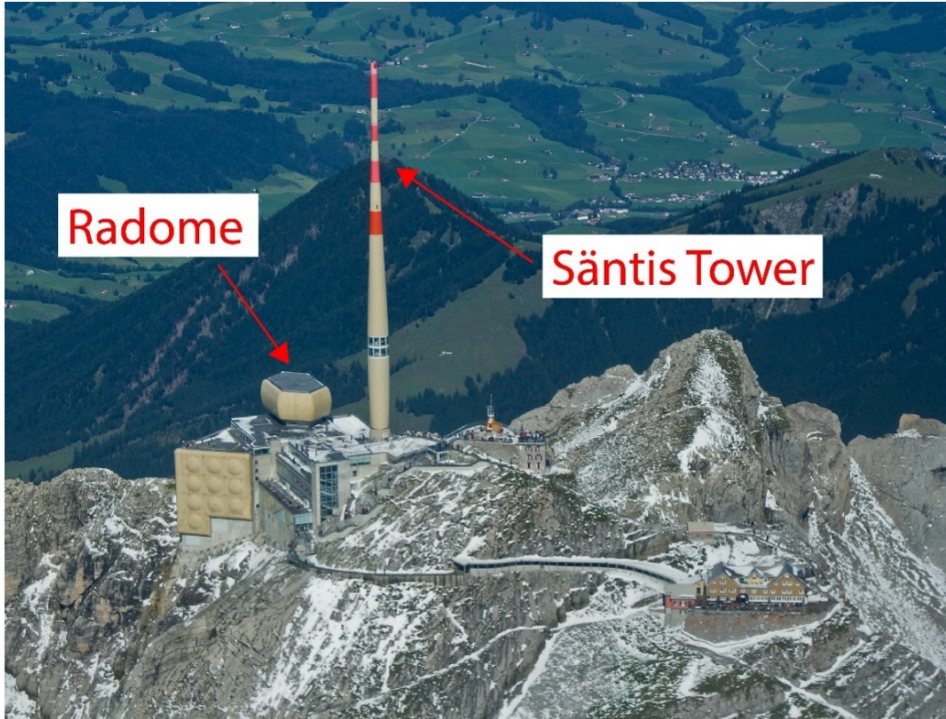


Figure 1: Photo of the Sântis peak, with arrows indicating the Radome, which houses an electric field probe, and the Tower, where the current sensors are located. Image reproduced from Rachidi and Rubinstein (2022) (Fig. 2) with permission.

Winn et al. (2012) suggested that only one mode of charge transfer exists for ICC pulses: the attachment of a dart leader on a relatively dark branch to an illuminated branch. Warner et al. (2012) presented a similar picture, stating in addition that the dart leader attached to the actively luminous main channel that was already connected to the top of a tall object. The dart leader was moreover observed to be a bidirectional recoil leader. Yoshida et al. (2012) observed, in agreement with the above, that the ICC pulses can indeed be the result of the connection of recoil leaders to the main active channel, but they also observed, using VHF images, that ICC pulses can also be associated with stepped leaders in the cloud that attach to a current-carrying channel connected to ground in triggered lightning.

Heretofore, mixed-mode ICC pulses have only been observed in upward negative flashes. Herein, we report, to the best of our knowledge, the first observation of the mixed mode of charge transfer during an upward *positive* flash, which was initiated from the Sântis Tower in Switzerland, and propose this as the physical mechanism responsible for the “main pulse” observed in some upward positive flashes.

2 Materials & Methods / Experimental Setup

The Mt. Sântis Lightning Research Facility, shown in Figure 1, is situated at 2502 m ASL in the Appenzell Alps of north-eastern Switzerland, and experiences >100 direct lightning strikes per year to its 124 meter-tall tower, which is equipped with a comprehensive current measurement system consisting of Rogowski coil and B-dot sensor pairs at two different heights: 24 and 82 meters above ground level (AGL). The nearby Radome (20 m from the Tower base) houses an E-field sensor with a sampling rate of 20 MHz.

This M elop ee fast E-field probe has a frequency range of 1 kHz to 150 MHz and is described in more detail in Sunjerga, Mostajabi, et al. (2021). Five kilometers away, atop Mt. Kr onberg (1663 m ASL), is a high-speed camera (HSC) operating at 24,000 fps, with an exposure time of $\sim 41 \mu\text{s}$ and a resolution of 512×512 pixels. Electric field measurements are also taken 15 km away by a flat-plate antenna with line-of-sight in Herisau, Switzerland, which has a frequency range of 40 Hz to 40 MHz and a time constant of 4 ms.

Additionally, during the Summer of 2021, when the flash discussed below occurred, a second high-speed camera operating at 11,500 fps with 512×512 pixel resolution was installed in Schw agalp, at the base of Mt. S antis (line-of-sight distance of ~ 2 km from the Tower), and was used in conjunction with the Kr onberg HSC to estimate the 3D velocities of the upward negative leader.

The Radome E-field signal is synchronized with the tower current signal by aligning the time of the first E-field “step” with the time of the first current pulse, i.e., the first significant deviation from zero in both waveforms, associated with the onset of the upward negative leader and the ICC, respectively. The high-speed cameras and “far” E-field data are synchronized with the rest by GPS timestamp if the antennae are functional at the time of the flash. If not, manual synchronization can be carried out via waveform matching. More detailed information on the S antis measurement system can be found in Rachidi and Rubinstein (2022).

All computational data analysis and presentation were carried out using MATLAB and the Python programming language, in particular the NumPy, SciPy, and Matplotlib libraries.

3 Results / Observations

The upward positive flash observed and analyzed in this study initiated from the S antis Tower at 16:24:03 UTC on July 24th, 2021. The integrated high-speed camera frames, as well as the current and electric field waveforms, for the whole flash are shown in Figure 2. In the right-hand panel of Figure 2, one can discern the S antis tower, from which the flash initiated, at the base of the rather tortuous plasma channel.¹ A superposed red arrow indicates the 2D distance from the tower tip to the junction point, where a downward-propagating leader connected to the conducting portion of the plasma channel, after retracing a decayed channel. The tower current waveform (top left panel) features the ICC associated with the upward negative leader, which lasted for 13.45 ms before being punctuated by a “return stroke”-like main pulse, followed by a couple minor M-component-type pulses, then a gradually-decaying current. The close electric field (Radome, 20 m) waveform in the middle left panel features large changes associated with the upward negative leader, whose stepping also produced small pulses in the 15 km electric field waveform (lower left panel), though these are not visible at this scale; see Figure 3. The “return stroke”-like main pulse is also present in the E-field waveforms, albeit to a lesser degree in the Radome. Note that the large changes midway through the 15-km Herisau E-field waveform are likely due to unrelated nearby lightning activity. Highlighted by dotted vertical red lines in all three Figure 2 waveforms are the three phases of greatest interest: (a) initiation of the upward negative leader, (b) creation of the plasma channel branch along which the recoil leader will later propagate, and (c) the main pulse following the connection of the recoil leader to the current carrying channel.

Figure 3 provides a close-up of phase (a). We observe the characteristic ICC pulses and electric field changes associated with the creation and propagation of an upward negative stepped leader. These are attenuated over time due to signal propagation effects,

¹ The faint black streak running diagonally across the integrated stills is formed by raindrops beading on the camera’s protective windowpane.

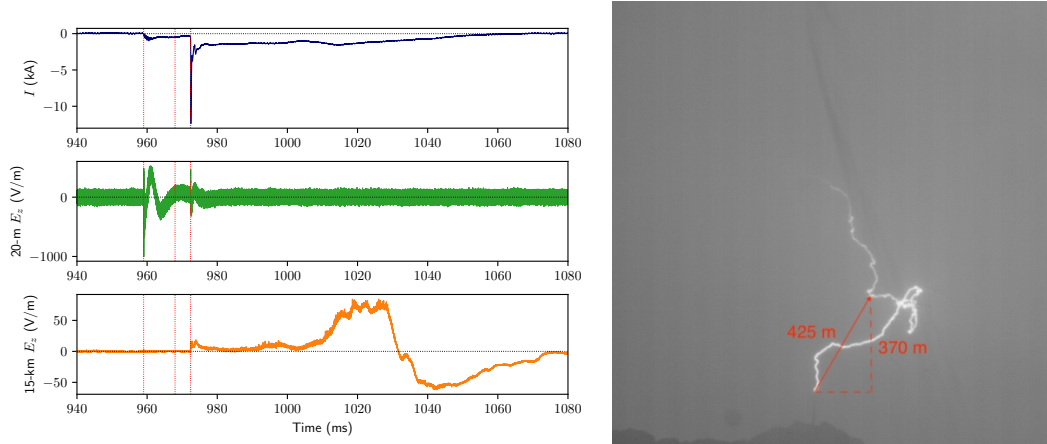


Figure 2: Waveforms (current, near and “far” E-field) of the observed upward positive flash that occurred on July 24, 2021 at 16:24:03 UTC. Top left waveform: tower current. A 100 kHz low-pass filter was applied to remove intermittent noise (though the current peak and rise time were determined from the raw data), and we chose the sign convention of a negative current corresponding to a positive charge transfer from cloud to ground. Middle and bottom left waveforms: measured vertical electric field at 20 m (Radome) and 15 km (Herisau), respectively. The Herisau E-field was manually synchronized with the other two waveforms, and therefore accounts for the $\sim 50 \mu\text{s}$ time delay. Time is measured from the beginning of the recording (~ 1 s before the current peak). The vertical red lines highlight the three phases of interest (from left to right: upward negative leader, recoil leader-channel creation, and main pulse) further analyzed in figures 3-5. The image on the right is an HSC-frame integration over the duration of the flash. Superposed red lines identify the 2D distances discussed in-text.

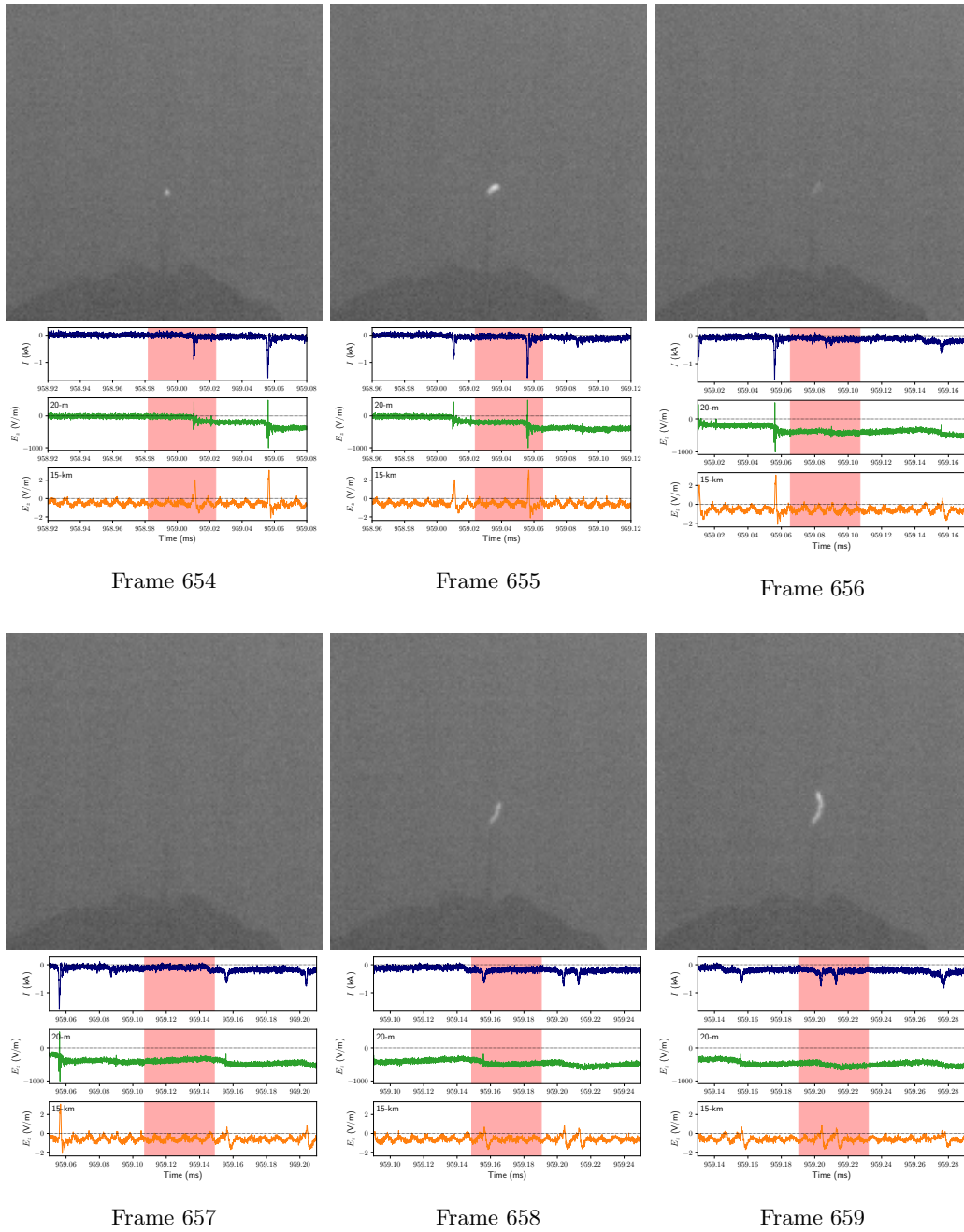


Figure 3: The upward negative stepped leader phase of the flash. The first six HSC frames are shown above. Their approximate temporal widths ($\sim 42 \mu\text{s}$) are highlighted by the red-shaded regions in the waveforms below, which depict, from top to bottom, the tower current (blue), 20-m E-field (green), and 15-km E-field (orange), as before. See Oregel-Chaumont, Šunjerga, Hettiarachchi, et al. (2024) for a detailed discussion of this phase, and Figure 2 for a zoomed-out view of the waveforms.

but the baseline current and near E-field continue to increase as the plasma channel extends (this static component is lost in the far-field, though the radiated “steps” remain distinguishable).

Figure 4 provides a close-up of phase (b): the branch-creation process. We see from the HSC frames how this new plasma channel extends from the junction point, reflected in the waveforms as a steady continuous current and non-zero electric field. Yellow dashed ellipses highlight the lengthening branch in each frame. The prior formation of this plasma channel provides evidence that the main pulse to come was preceded by specifically a recoil leader.

Mazur (2002) defined recoil leaders as negative leaders traversing preexisting positive channels. In 2019, Qie et al. (2019) observed for the first time the inverse case: positive recoil leaders with a positive leader tip retrograding in a preexisting negative channel. This is also the case for the presented flash in our study, as observed in Figure 5, which provides a close-up of phase (c). These high-speed camera frames confirm that the main pulse of this particular upward positive flash was triggered by a downward-connecting recoil leader with a 2D junction height of 370 ± 5 m above the tower tip (see Figure 2), well below the 1 km cutoff suggested by Zhou et al. (2015) for pulses to be classified as mixed-mode pulses. The tower current and near E-field waveforms, though expectedly non-zero, display very little change until the connection time, at which point a large current wave propagates from the junction point (Frame 976). Note that the fast pulses leading up to the main pulse in the 15-km Herisau E-field waveform (Frames 972–975) may indeed be due to the recoil leader, implying a stepped nature. Their absence in the Radome (near) field can be explained by the Azadifar et al. (2019) model for M-components in upward flashes: the Distance Range Ratio (DRR) they define “as the ratio of the peak amplitudes of the microsecond-scale pulse at the start of the M-component and of the ensuing millisecond-scale pulse”, was shown to be directly proportional to distance, such that these fast (μ s-scale) pulses associated with the branch current wave vanish in the near field. Physically-speaking, this is due to their being overwhelmed by the static component of the electric field, which is negligible at a distance of 15 km. The distinction here is that our observed fast pulses are associated with a recoil leader current wave *descending* the branch *prior* to the connection time, as opposed to the Azadifar et al. (2019) model’s current wave *ascending* the branch *post*-connection.

Interestingly, while the observed main pulse’s 12 kA peak current is reasonable for a mixed-mode pulse, the current and E-field rise times are both $>10 \mu$ s, more characteristic of an M-component-type ICC pulse (Flache et al., 2008), see Frame 976 of Figure 5. This might be due to signal propagation along the plasma channel (2D length of >730 m from the tower tip to the junction point), as opposed to through the air (~ 425 m), which results in an increase in the current rise time, and subsequently the E-field rise time. These lengths were estimated from the Krönberg HSC (as the Schwägalp HSC’s field of view was limited to the bottom of the channel); dividing the former by the time it took for the upward negative leader to reach the junction point, the average 2D velocity of the upward negative leader was estimated to be $\sim 9 \times 10^4$ m/s. This is on the lower end of the range established by Wu et al. (2020) for 3D horizontal propagation: 0.9 to 7.3×10^5 m/s with a mean value of 3.8×10^5 m/s. Although the Schwägalp HSC’s sensitivity was set to capture return strokes, too low to observe the upward negative leader-stepping phase of the flash depicted in Figure 3, we were able to reconstruct the 3D geometry of the bottom of the channel from overlapping fields-of-view using later-time frames, and subsequently estimate the 3D leader velocity to be $\sim 2.4 \times 10^5$ m/s from the early-time Krönberg HSC frames, such as those presented in Figure 3. This aligns much better with the 3D speeds of Wu et al. (2020), both for horizontal propagation (discussed above), as well as vertical propagation: 1.8 to 27.9×10^5 m/s, albeit lower than their mean value of 10.4×10^5 m/s. In turn, we can multiply our new velocity by the time (~ 8.38 ms) between the onset of the ICC (Figure 3) and the creation of the future re-

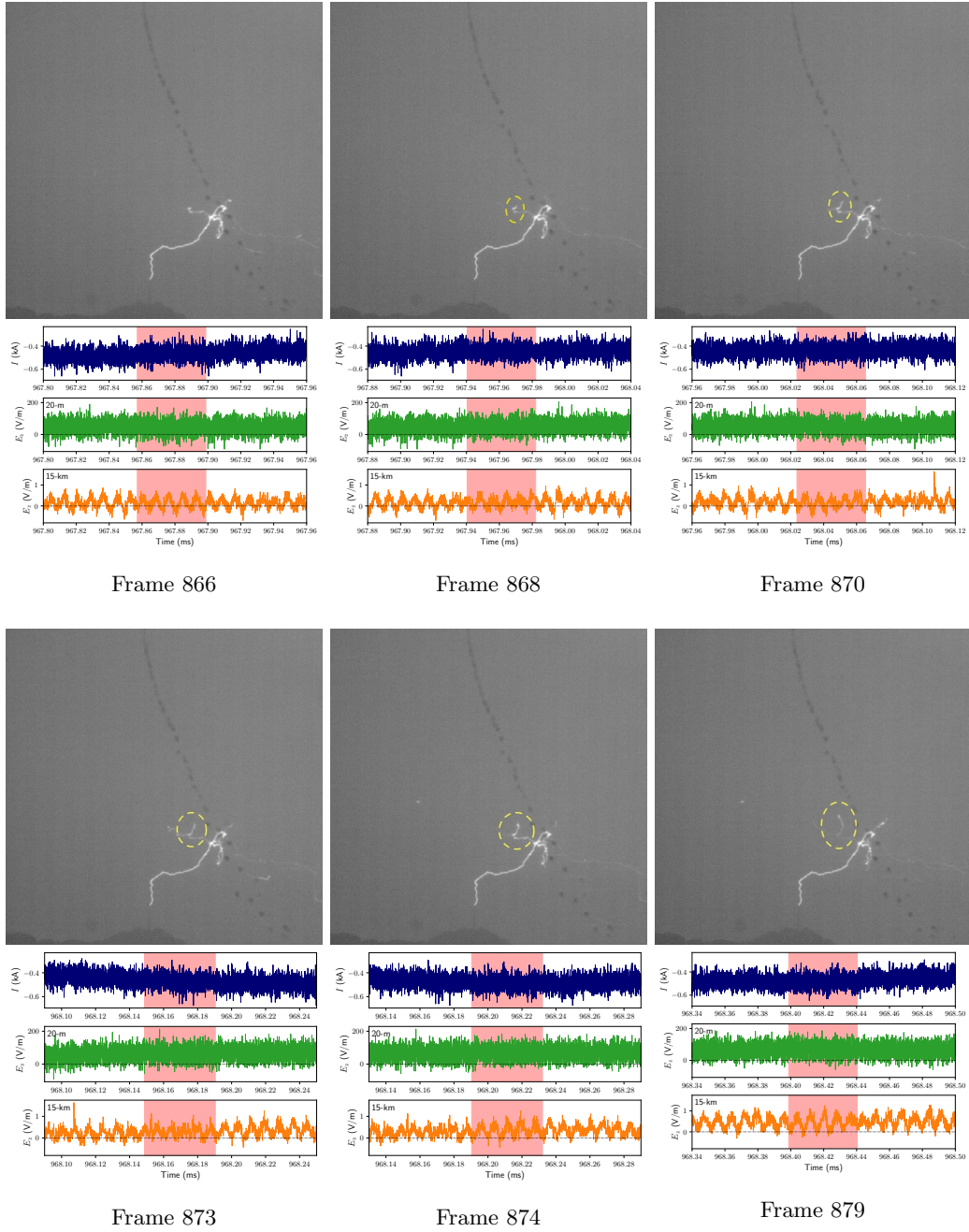


Figure 4: The creation of the plasma channel (2D junction height of 495 ± 5 m AGL) along which the recoil leader will later propagate (highlighted in light blue). See Figure A1 for more frames and details. The waveforms are as described in Figure 3.

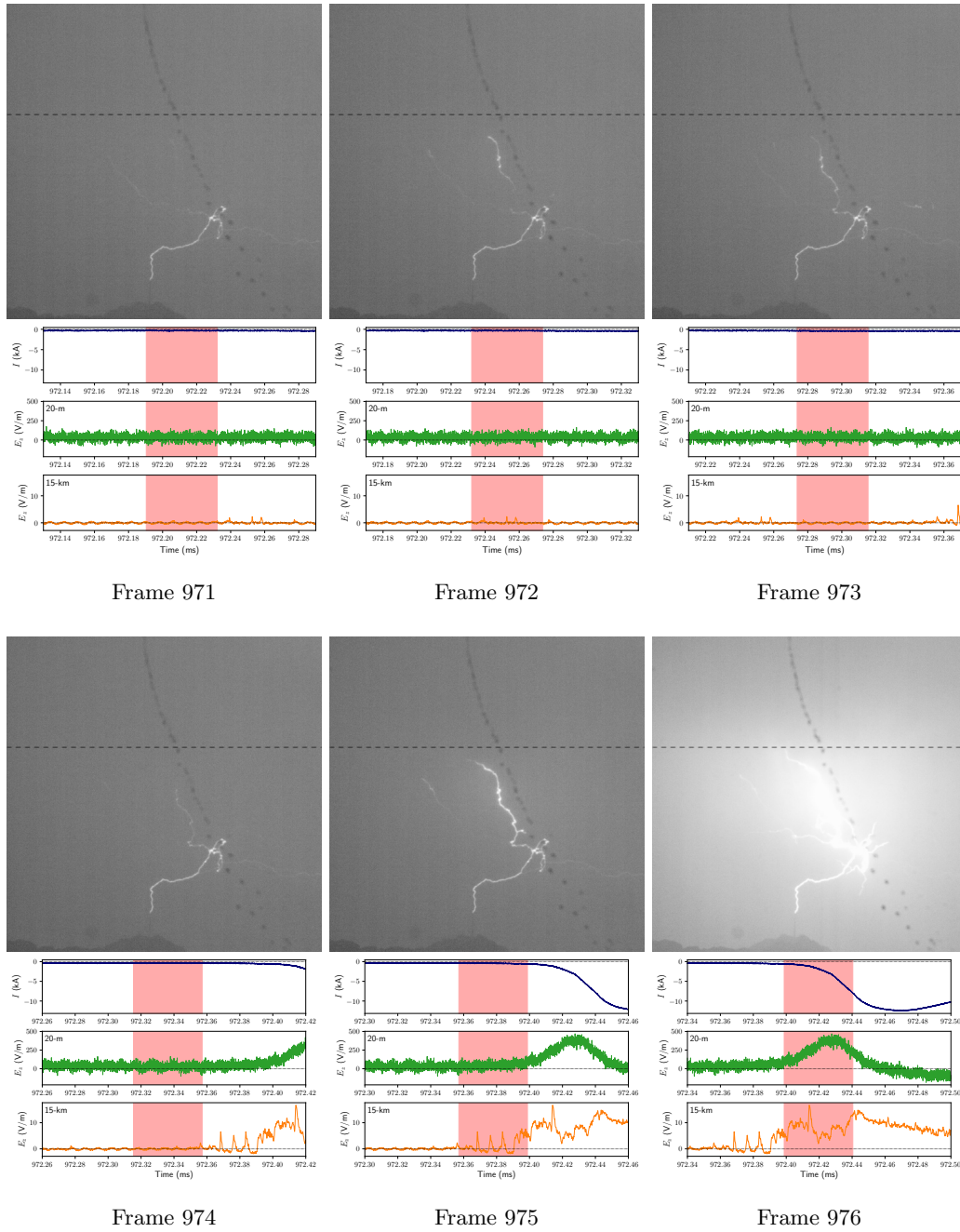


Figure 5: The lead-up to the main pulse of the flash, which occurred 13.45 ms after the onset of the ICC. The six HSC frames leading up to the arrival of the recoil leader at the junction point are shown above. A dashed, horizontal line has been added to identify the approximate cloud base (~ 900 m above the tower). The waveforms are as described in Figure 3.

Table 1: Main pulse characteristics

t_{SL} [ms]	Junction [m]		I_p [kA]	t_{10-90} [μ s]	ΔE [$\frac{V}{m}$]		t_{Er} [μ s]		t_{lag} [μ s]	AsWC
	2D Height	3D Length			20 m	15 km	20 m	15 km		
13.45	370 \pm 5	\sim 2010	12.10 \pm 0.05	\sim 15	470 \pm 40	16.4 \pm 0.3	\sim 40	\sim 20	\sim 40	0.84

coil leader’s branch, depicted in figures 4 & A1, to more accurately estimate the 3D tower-tip-to-junction-point channel length as \sim 2010 m.

Analysis of frames 972 through 975 in Figure 5 can approximate the downward propagation velocity (2D average) of the recoil leader to be $\sim 4 \times 10^6$ m/s. This is over an order of magnitude faster than most previous estimates of positive leader speeds. Biagi et al. (2010) and Jiang et al. (2014) calculated the 2D velocities of rocket-triggered upward positive leaders to be in the range of $0.55\text{--}1.8 \times 10^5$ m/s. Montanyà et al. (2015) observed a “virgin air” bidirectional leader, and determined its positive end to propagate with a (decreasing) speed of $1 - 9 \times 10^4$ m/s. An analysis by Wu et al. (2020) of negative cloud-to-ground and intra-cloud flashes found positive leader velocities around $1\text{--}3 \times 10^4$ m/s. Our observed 2D partial speed was comparable, however, to that measured by Qie et al. (2019) for the positive end of a bidirectional recoil leader in an upward positive flash of Type 2 (as defined by Romero et al. (2013); see next section), at 6.4×10^6 m/s. In their study, the observed positive tip propagated upwards into the cloud, while the negative tip propagated downwards, eventually connecting to the main (upward negative) leader channel. Considering our upward positive flash was of Type 1, and it was the *positive* leader tip that connected to the main leader channel, we propose this unique configuration of charge transfer as the triggering mechanism for the characteristic main pulse.

It should also be noted that this flash occurred during the Laser Lightning Rod project presented in Houard et al. (2023) (therein labelled L2), while the laser was on. The guiding effect discussed therein was confined to early-stage propagation, only observed over a distance of about 50 m (see their Fig. 2), and therefore should not have impacted the effects studied in this article, which occurred an order of magnitude higher. See Oregel-Chaumont, Šunjerga, Hettiarachchi, et al. (2024) for further discussion.

4 Discussion

Romero et al. (2013) classified upward positive flashes into two categories: Type 1 flashes, which exhibit a large unipolar return stroke-like current pulse following the upward negative stepped-leader phase, and Type 2 flashes, which do not feature such a large pulse and consist solely of a 100 millisecond-scale waveform with large, oscillatory pulse trains due to upward negative stepped leaders. From the waveforms presented in figures 2 & 5, our flash was clearly a Type 1 upward positive flash; the characteristics of its Main Pulse are summarized in Table 1: (from left to right) the time from the onset of the stepped leader, the junction height and length, the absolute value peak current, the current pulse 10-90% rise time, the associated near and far electric field changes and rise times, the time lag between the current and the 20-m electric field, and the asymmetrical waveform coefficient of the current pulse, as defined in He et al. (2018), see below.

The classification scheme of Romero et al. (2013) was based exclusively on current waveform observations. The analysis presented in the present paper allows us to propose a physical mechanism describing Type 1 and Type 2 positive flashes, as illustrated in Fig-

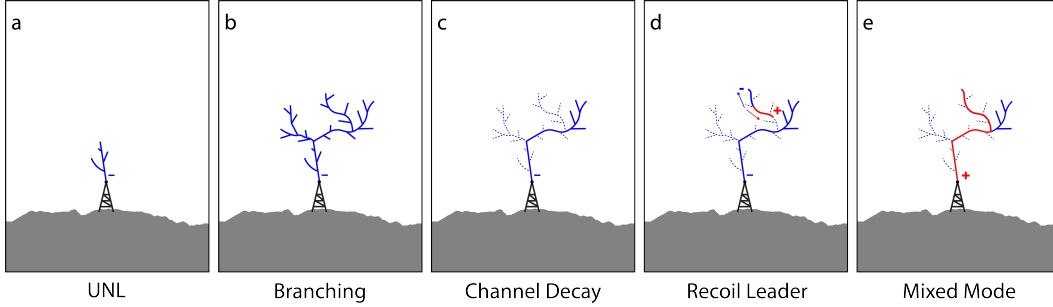


Figure 6: Diagram depicting the underlying mechanisms in a typical upward positive flash. Blue and red indicate negative and positive charge transfer, respectively, while solid and dashed lines indicate active and decayed branches, respectively. Type 2 flashes end after the third phase (c), i.e., the current gradually dies out as the plasma channels decay. The main pulse in Type 1 flashes is due to the connection of a positive recoil leader with the main branch, as illustrated in (d) and (e).

Table 2: Existing criteria for distinguishing MM and M-C type ICC pulses

Type	Junction height [km] (Zhou et al., 2015)	t_{10-90} [μ s] (Flache et al., 2008)	t_{lag} [μ s] (Zhou et al., 2015)	AsWC (He et al., 2018)
MM	< 1	< 8	< 10	> 0.8
M-C	> 1	> 8	> 10	< 0.8

Figure 6. Both types begin with (a) an upward negative leader (UNL) initiated at the tip of the strike object, which undergoes significant branching (b) as it rises towards the cloud. Most of these branches decay (c), leaving a main, current-carrying channel. This is where it ends for Type 2 upward positive flashes. Type 1 flashes, however, see a (possibly stepped and bidirectional) recoil leader descending a defunct plasma channel (d), to reconnect with the main branch, triggering their characteristic main pulse (e) which propagates from the junction point.

The high-speed camera frames in Figure 4 presented earlier-time evidence of the existence of the plasma channel later retraced by the recoil leader. It can be seen from the waveforms in Figure 5 that this recoil leader (possibly bidirectional, though the ascending negative tip is not visible if so) initiated a mixed-mode charge transfer of positive polarity, as inferred from the signs of the current pulse and associated E-field changes. It is of interesting note that positive recoil leaders should play a role in upward positive flashes, in a similar way as Sunjerga, Rubinstein, et al. (2021) demonstrated that *negative* recoil leaders play a role in upward *negative* flashes.

As discussed in Section 1, Zhou et al. (2015) also used the time between the field and the current to distinguish between M-component type and mixed-mode pulses, which is equivalent to a height criterion of the attachment point of the rejuvenated branch attaching to the main channel. Table 2 presents the distinction criteria proposed in the literature: ‘MM’ and ‘M-C’ stand for mixed-mode and M-component -type ICC pulses, respectively; t_{10-90} is the 10–90% current rise time in microseconds (Flache et al., 2008);

Table 3: Classification of the main pulse as either Mixed Mode (MM) or M-component-type ICC pulse, based on the existing criteria

Junction		I_p	t_{10-90}	t_{lag}	AsWC
2D Height	3D Length				
MM	M-C	MM	M-C	M-C	MM

t_{lag} the time lag between the current and E-field peaks in microseconds (Zhou et al., 2015)²; and AsWC the asymmetrical waveform coefficient of the current pulse, defined by He et al. (2018) as:

$$\text{AsWC} = \frac{\text{FWHM} - t_{50-100}}{\text{FWHM}} \quad (1)$$

where FWHM and t_{50-100} are the full width at half maximum and 50–100% rise time, respectively. Note that the criteria presented by Zhou et al. (2015) are based on the implicit assumption of a vertical channel. Since the main plasma channel of the flash discussed here exhibited significant tortuosity with a substantial horizontal component, the tower-tip-to-junction-point length may be a better criterion than the junction height. To this point, Table 3 shows how the characteristics of the observed flash’s main pulse are such that it could be classified as either a mixed-mode or M-component -type ICC pulse, depending on which criterion is considered. Specifically, the 2D junction height of 370 m and $\text{AsWC} \approx 0.84$ would classify it a mixed mode,³ while the 3D channel length of 2 km, the $t_{10-90} \approx 15 \mu\text{s}$, and the $t_{lag} \approx 40 \mu\text{s}$, all seem to suggest an M-component-type.

As discussed in Section 1, since both modes involve the continuous current mode of charge transfer in addition to a second mode of charge transfer (M-component-type or return stroke-like), the term “mixed mode” applied to only one type of pulses may not be the optimum choice as further discussed below. If we assume that branches can indeed attach to the channel at any height, then a gradual transition between these wave shapes should be observable. The terms M-component type and mixed mode, applied to cases in which the attachment point is, respectively, far or close to the channel base, may therefore not fully capture the spectrum of behaviors observed, as one would expect a continuum of pulse rise times and symmetries that vary with the junction height (or the length of the channel to the attachment point).

5 Conclusions

Herein we provided a physical mechanism distinguishing Type 1 and Type 2 upward positive flashes. We have shown that the Type 1 main current pulse can be the result of a recoil leader-initiated mixed mode of charge transfer, determined by the current and electric field records to be of positive polarity, the first inference of its kind. The estimated propagation speed of this recoil leader’s positive tip was consistent with prior measurements, but unique in being the first observation in a Type 1 upward positive flash. Furthermore, the recoil leader was accompanied by a series of fast electric field pulses that suggest step-like propagation: to our knowledge another observational first. More data are needed to confirm that the proposed mechanism is the only one describing a

²Note that this value depends on the E-field measurement distance; Zhou et al. (2015) based their 10 μs cutoff on the Rakov et al. (1995) 30 m, whereas our sensor is at 20 m. This is an acceptable difference as the junction point is over an order of magnitude further away.

³Note the proximity of our calculated AsWC to the defined 0.8 cutoff.

Type 1 flash. These observations contribute to improving our understanding of the mechanisms of charge transfer in upward lightning flashes, and will be furthered by in-depth analysis of differences between the various types.

Appendix A Branching HSC Frames

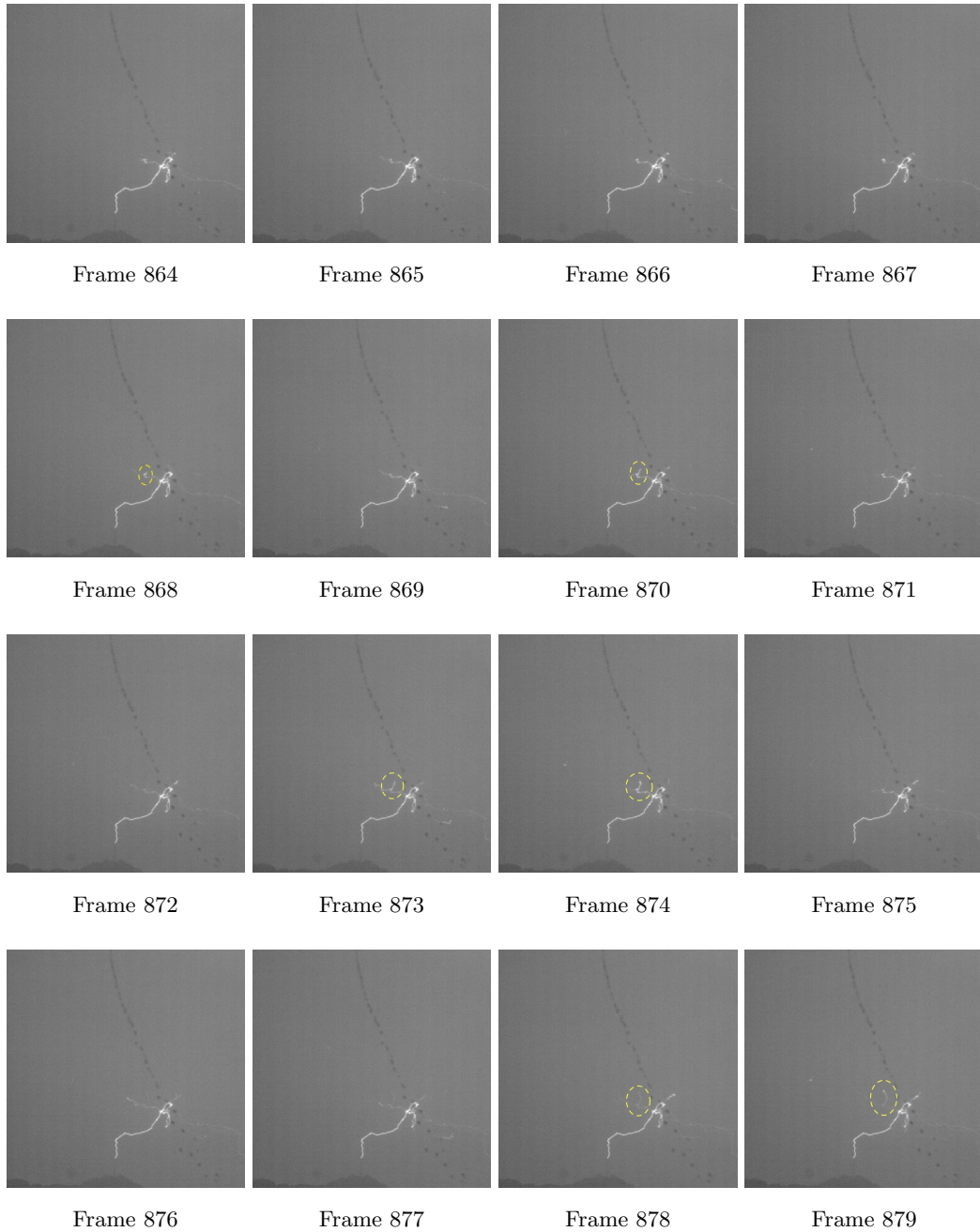


Figure A1: HSC frames showing the creation of the plasma channel (2D junction height of 495 ± 5 m AGL) along which the recoil leader will later propagate. The branch first appears noticeably in Frame 868, and further demonstrates significant propagation in Frames 870, 873, 874, 878, and 879 (highlighted in yellow). The time between two consecutive frames is $\sim 42 \mu\text{s}$.

Open Research

All processed data analysed during this study are included in this published article. Raw data sets and code are available from Oregel-Chaumont, Šunjerga, Kasparian, et al. (2024) in Zenodo (DOI: 10.5281/zenodo.14035777) and GitHub (<https://github.com/TomaOC/santis>), respectively.

Acknowledgments

This work was supported in part by the Swiss National Science Foundation (Project nos. 200020_175594 and 200020_204235) and the European Union’s Horizon 2020 research and innovation program (grant agreement no. 737033-LLR). The authors would like to thank Florent Aviolat for developing a data-visualisation software that expedited flash analysis.

References

- Azadifar, M., Rubinstein, M., Li, Q., Rachidi, F., & Rakov, V. (2019, December). A New Engineering Model of Lightning M Component That Reproduces Its Electric Field Waveforms at Both Close and Far Distances. *J. Geophys. Res. Atmos.*, *124*(24), 14008–14023. Retrieved 2022-07-01, from <https://onlinelibrary.wiley.com/doi/10.1029/2019JD030796> doi: 10.1029/2019JD030796
- Biagi, C. J., Uman, M. A., Hill, J. D., Jordan, D. M., Rakov, V. A., & Dwyer, J. (2010, December). Observations of stepping mechanisms in a rocket-and-wire triggered lightning flash. *J. Geophys. Res.*, *115*(D23), 2010JD014616. Retrieved 2023-11-09, from <https://agupubs.onlinelibrary.wiley.com/doi/10.1029/2010JD014616> doi: 10.1029/2010JD014616
- Flache, D., Rakov, V. A., Heidler, F., Zischank, W., & Thottappillil, R. (2008, July). Initial-stage pulses in upward lightning: Leader/return stroke versus M-component mode of charge transfer to ground. *Geophysical Research Letters*, *35*(13), 2008GL034148. Retrieved 2023-12-15, from <https://agupubs.onlinelibrary.wiley.com/doi/10.1029/2008GL034148> doi: 10.1029/2008GL034148
- He, L., Azadifar, M., Rachidi, F., Rubinstein, M., Rakov, V. A., Cooray, V., . . . Xing, H. (2018, April). An Analysis of Current and Electric Field Pulses Associated With Upward Negative Lightning Flashes Initiated from the Sântis Tower. *J. Geophys. Res. Atmos.*, *123*(8), 4045–4059. Retrieved 2022-05-16, from <https://onlinelibrary.wiley.com/doi/10.1029/2018JD028295> doi: 10.1029/2018JD028295
- Houard, A., Walch, P., Produit, T., Moreno, V., Mahieu, B., Sunjerga, A., . . . Wolf, J.-P. (2023, March). Laser-guided lightning. *Nat. Photon.*, *17*(3), 231–235. Retrieved 2023-08-16, from <https://www.nature.com/articles/s41566-022-01139-z> doi: 10.1038/s41566-022-01139-z
- Jiang, R., Wu, Z., Qie, X., Wang, D., & Liu, M. (2014, July). High-speed video evidence of a dart leader with bidirectional development: BIDIRECTIONAL DEVELOPMENT OF DART LEADER. *Geophys. Res. Lett.*, *41*(14), 5246–5250. Retrieved 2022-05-25, from <http://doi.wiley.com/10.1002/2014GL060585> doi: 10.1002/2014GL060585
- Li, Q., Azadifar, M., Rubinstein, M., Rachidi, F., Nucci, C. A., Wang, J., & He, J. (2023, February). A review of the modeling approaches of the lightning M-component with special attention to their current and electric field characteristics. *Electric Power Systems Research*, *215*, 108977. Retrieved 2024-06-04, from <https://linkinghub.elsevier.com/retrieve/pii/S0378779622010264> doi: 10.1016/j.epsr.2022.108977
- Mazur, V. (2002, October). Physical processes during development of light-

- ning flashes. *Comptes Rendus. Physique*, 3(10), 1393–1409. Retrieved 2024-06-17, from [https://comptes-rendus.academie-sciences.fr/physique/articles/10.1016/S1631-0705\(02\)01412-3/](https://comptes-rendus.academie-sciences.fr/physique/articles/10.1016/S1631-0705(02)01412-3/) doi: 10.1016/S1631-0705(02)01412-3
- Montanyà, J., Van Der Velde, O., & Williams, E. R. (2015, October). The start of lightning: Evidence of bidirectional lightning initiation. *Sci Rep*, 5(1), 15180. Retrieved 2024-02-29, from <https://www.nature.com/articles/srep15180> doi: 10.1038/srep15180
- Oregel-Chaumont, T., Šunjerga, A., Hettiarachchi, P., Cooray, V., Rubinstein, M., & Rachidi, F. (2024, April). Direct observations of X-rays produced by upward positive lightning. *Sci Rep*, 14(1), 8083. Retrieved 2024-05-05, from <https://www.nature.com/articles/s41598-024-58520-x> doi: 10.1038/s41598-024-58520-x
- Oregel-Chaumont, T., Šunjerga, A., Kasparian, J., Rubinstein, M., & Rachidi, F. (2024, November). *Säntis upward positive flash 2021-07-24 at 16:24 UTC*. Zenodo. doi: 10.5281/zenodo.14035777
- Qie, X., Yuan, S., Zhang, H., Jiang, R., Wu, Z., Liu, M., ... , Fujian Meteorological Service Center, Fujian Meteorological Bureau, Fuzhou 350001, China (2019). Propagation of positive, negative, and recoil leaders in upward lightning flashes. *Earth and Planetary Physics*, 3(2), 102–110. Retrieved 2024-06-20, from <http://www.epscgs.org//article/doi/10.26464/epp2019014?pageType=en> doi: 10.26464/epp2019014
- Rachidi, F., & Rubinstein, M. (2022, June). Säntis lightning research facility: a summary of the first ten years and future outlook. *Elektrotech. Inftech.*, 139(3), 379–394. Retrieved 2023-07-02, from <https://link.springer.com/10.1007/s00502-022-01031-2> doi: 10.1007/s00502-022-01031-2
- Rakov, V. A., Thottappillil, R., Uman, M. A., & Barker, P. P. (1995). Mechanism of the lightning M component. *J. Geophys. Res.*, 100(D12), 25701. Retrieved 2022-07-04, from <http://doi.wiley.com/10.1029/95JD01924> doi: 10.1029/95JD01924
- Romero, C., Rachidi, F., Rubinstein, M., Paolone, M., Rakov, V. A., & Pavanello, D. (2013, December). Positive lightning flashes recorded on the Säntis tower from May 2010 to January 2012: POSITIVE LIGHTNING SÄNTIS TOWER. *J. Geophys. Res. Atmos.*, 118(23), 12,879–12,892. Retrieved 2023-05-01, from <http://doi.wiley.com/10.1002/2013JD020242> doi: 10.1002/2013JD020242
- Sunjerga, A., Mostajabi, A., Paolone, M., Rachidi, F., Romero, C., Hettiarachchi, P., ... Smith, D. (2021, September). Säntis Lightning Research Facility Instrumentation. *ICLP*, 6.
- Sunjerga, A., Rubinstein, M., Azadifar, M., Mostajabi, A., & Rachidi, F. (2021, September). Bidirectional Recoil Leaders in Upward Lightning Flashes Observed at the Säntis Tower. *JGR Atmospheres*, 126(18). Retrieved 2022-05-19, from <https://onlinelibrary.wiley.com/doi/10.1029/2021JD035238> doi: 10.1029/2021JD035238
- Warner, T. A., Cummins, K. L., & Orville, R. E. (2012, October). Upward lightning observations from towers in Rapid City, South Dakota and comparison with National Lightning Detection Network data, 2004–2010. *J. Geophys. Res.*, 117(D19), 2012JD018346. Retrieved 2024-09-24, from <https://agupubs.onlinelibrary.wiley.com/doi/10.1029/2012JD018346> doi: 10.1029/2012JD018346
- Winn, W. P., Eastvedt, E. M., Trueblood, J. J., Eack, K. B., Edens, H. E., Aulich, G. D., ... Murray, W. C. (2012, May). Luminous pulses during triggered lightning. *J. Geophys. Res.*, 117(D10), 2011JD017105. Retrieved 2024-09-24, from <https://agupubs.onlinelibrary.wiley.com/doi/10.1029/2011JD017105> doi: 10.1029/2011JD017105

- Wu, T., Wang, D., & Takagi, N. (2020, August). Upward Negative Leaders in Positive Upward Lightning in Winter: Propagation Velocities, Electric Field Change Waveforms, and Triggering Mechanism. *J. Geophys. Res. Atmos.*, *125*(16). Retrieved 2023-01-13, from <https://onlinelibrary.wiley.com/doi/10.1029/2020JD032851> doi: 10.1029/2020JD032851
- Yoshida, S., Biagi, C. J., Rakov, V. A., Hill, J. D., Stapleton, M. V., Jordan, D. M., ... Akita, M. (2012, May). The initial stage processes of rocket-and-wire triggered lightning as observed by VHF interferometry. *J. Geophys. Res.*, *117*(D9), 2012JD017657. Retrieved 2024-09-24, from <https://agupubs.onlinelibrary.wiley.com/doi/10.1029/2012JD017657> doi: 10.1029/2012JD017657
- Zhou, H., Diendorfer, G., Thottappillil, R., Pichler, H., & Mair, M. (2011, November). Mixed mode of charge transfer to ground for initial continuous current pulses in upward lightning. In *2011 7th Asia-Pacific International Conference on Lightning* (pp. 677–681). Chengdu, China: IEEE. Retrieved 2023-12-14, from <http://ieeexplore.ieee.org/document/6110212/> doi: 10.1109/APL.2011.6110212
- Zhou, H., Rakov, V. A., Diendorfer, G., Thottappillil, R., Pichler, H., & Mair, M. (2015, April). A study of different modes of charge transfer to ground in upward lightning. *Journal of Atmospheric and Solar-Terrestrial Physics*, *125-126*, 38–49. Retrieved 2022-05-13, from <https://linkinghub.elsevier.com/retrieve/pii/S1364682615000413> doi: 10.1016/j.jastp.2015.02.008